Dynamics of sessile and pendant drops excited by surface acoustic waves: Gravity effects and correlation between oscillatory and translational motions

Adrien Bussonnière, Michael Baudoin, Philippe Brunet, Olivier Bou Matar

Dynamics of sessile and pendant drops excited by surface acoustic waves: Gravity effects and correlation between oscillatory and translational motions

A. Bussonnière,[1] M. Baudoin,[1,*] P. Brunet,[2] and O. Bou Matar[1]

[1]*Université Lille 1, International Laboratory LEMAC/LICS, IEMN, UMR CNRS 8520, Avenue Poincaré, 59652 Villeneuve d'Ascq, France*

[2]*Laboratoire Matière et Systèmes Complexes, UMR CNRS 7057, Université Paris Diderot, 10 rue Alice Domon et Léonie Duquet, 75205 Paris cedex 13, France*

(Received 27 December 2015; published 12 May 2016)

When sessile droplets are excited by ultrasonic traveling surface acoustic waves (SAWs), they undergo complex dynamics with both oscillations and translational motion. While the nature of the Rayleigh-Lamb quadrupolar drop oscillations has been identified, their origin and their influence on the drop mobility remains unexplained. Indeed, the physics behind this peculiar dynamics is complex with nonlinearities involved both at the excitation level (acoustic streaming and radiation pressure) and in the droplet response (nonlinear oscillations and contact line dynamics). In this paper, we investigate the dynamics of sessile and pendant drops excited by SAWs. For pendant drops, so-far unreported dynamics are observed close to the drop detachment threshold with the suppression of the translational motion. Away from this threshold, the comparison between pendant and sessile drop dynamics allows us to identify the role played by gravity or, more generally, by an initial or dynamically induced stretching of the drop. In turn, we elucidate the origin of the resonance frequency shift, as well as the origin of the strong correlation between oscillatory and translational motion. We show that for sessile drops, the velocity is mainly determined by the amplitude of oscillation and that the saturation observed is due to the nonlinear dependence of the drop response frequency on the dynamically induced stretching.

DOI: 10.1103/PhysRevE.93.053106

I. INTRODUCTION

Surface acoustic waves (SAWs) are versatile tools for the actuation of fluids at small scales. In digital microfluidic, they can be used to move [1–3], divide [4], merge [5], atomize [6–11], mix [12], or heat [13–18] sessile droplets. In microchannels, they can induce fluid pumping [19,20] and mixing [21–23]. Finally, in both configurations, they can be used to manipulate and sort particles [24–31] and cells [26,32–38]. More recently, new types of surface acoustic waves, the so-called swirling waves (2D counterparts of Bessel beams) [39,40], have been under investigation to achieve new operations, such as 3D on-chip single-particle manipulation [41] or vortical flow synthesis with controlled topology [42].

However, despite an extensive literature on the use of SAW for labs-on-chips actuation [43–45], a clear understanding of the underlying physics is still missing for many of these systems [46]. One of the reasons is that the nonlinear coupling between the acoustic waves and the liquid response involves time and length scales that differ by several orders of magnitude, along with nonlinear effects, which render the analysis and simulation of these behaviors extremely difficult. A difficult problem is the physical understanding of droplets dynamics excited by planar propagative SAW. In this case the droplet undergoes both oscillatory and translational motion [3,47] that are strongly coupled to each other [48]. The droplet vibrations have been identified [3] to be inertiocapillary Rayleigh-Lamb quadrupolar oscillations, whose frequency f_{osc} is roughly 50 Hz, while the acoustic excitation is around $f_{\mathrm{saw}} = 20\,\mathrm{MHz}$. However, the origin of these oscillations [46,49] and their influence on the droplet translational motion [48] remain unexplained. As the SAW is radiated within the drop, it can generate both Eckart acoustic streaming and radiation pressure at the liquid-air interface. The relative contribution of these effects depends on the attenuation length of the wave in the liquid [3]. For a water droplet excited at 20 MHz, the wave attenuation length is typically around 10 cm compared to the drop size of a few millimeters and the wavelength of about 75 microns. Thus, the bulk attenuation is weak enough to allow for significant acoustic pressure to reach the interface and the radiation pressure acts by pushing the drop-free surface upwards, which leads to an average drop deformation and oscillations. Figure 1 shows a typical sequence for the dynamics for the drop, together with the geometrical definitions.

In this paper, we investigate the dynamics of sessile and pendant drops excited by Rayleigh-type SAW of frequency 20 MHz. It is shown that even for relatively small droplets, gravity strongly affects the drop dynamics. For pendant drops, new regimes are observed close to the detachment threshold with the appearance of a quasistatic equilibrium. Away from this threshold, the comparison of sessile and pendant drops dynamics allows us to identify the role played by gravity on the frequency f_{osc} and amplitude of oscillations Δh: since drops are nonlinear oscillators, their characteristic frequency relies on the average stretching of the string (here the drop shape). In the case of pendant drop, this stretching is mainly induced by stationary effects (gravity and radiation pressure) that both act in the same direction. For sessile drops, however, gravity and radiation pressure act in opposition and the average stretching is mainly induced by nonlinear dynamical effects, which depend on Δh. Thus, in this case f_{osc} is strongly influenced by Δh.

The motion of the contact line over one cycle is then analyzed for both pendant and sessile droplets. While the contact line dynamics is shown to depend also on gravity, it essentially remains a linear function of the amplitude

*michael.baudoin@univ-lille1.fr; http://films-lab.univ-lille1.fr

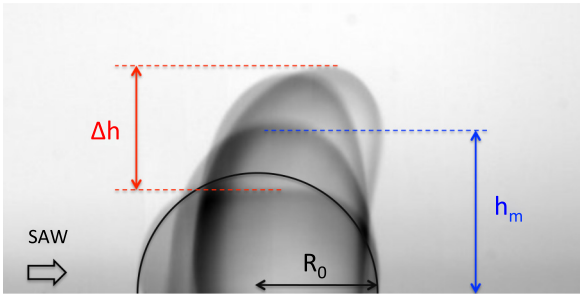

FIG. 1. Successive deformations of a drop excited by a Rayleigh SAW, leading to both translational motion at velocity V and oscillations of amplitude Δh and frequency $f_{\rm osc}$. The radiated acoustic wave leads to an average drop height h_m. The plain line circle and base radius R_o correspond to the shape without acoustic forcing.

of oscillations in both cases. As a consequence, both the frequency $f_{\rm osc}$ and the contact line motion over one cycle are directly dependent on the drop amplitude of oscillations for sessile droplets. In this case, it is thus possible to determine a relation between the droplet velocity V and the amplitude Δh. This equation quantitatively compares to the experimentally observed tendencies for all drop sizes, and in particular the saturation of the droplet velocity as a function of the amplitude of oscillation, previously observed in Ref. [48]. Consequently, it is shown that this saturation is mainly induced by the decrease of $f_{\rm osc}$ with Δh.

In Sec. II, the experimental setup is presented and the relevant dimensionless numbers are introduced. In Sec. III, we first analyze the motion and oscillation of both sessile and pendant drops and compare them in order to determine the effect of gravity. Finally, in Sec. IV the correlation between the droplet oscillations and translational motion is interpreted in light of previous results.

II. METHOD

A. Description of the setup

Sessile and pendant drop of deionized water are actuated by Rayleigh-type surface acoustic waves at driving frequency 20 MHz synthesized at the surface of a 1.05-mm-thick x-cut lithium niobate ($LiNbO_3$) piezoelectric surface in the z direction by interdigitated transducers (IDTs). The latter are excited by a high-frequency generator (IFR 2023A) and an Empower RF 1037 amplifier (see Fig. 2). The IDTs have been fabricated by successively sputtering a titanium (Ti) layer (20 nm thick) and a gold (Au) layer (200 nm thick) on the $LiNbO_3$ substrate. Spacing and width of the interdigitated fingers (both equal to $a = 43.75\,\mu$m in the present system) determine the frequency of the surface acoustic wave according to the law $f_{\rm saw} = c_s/\lambda = c_s/4a$, where $\lambda = 175\,\mu$m is the wavelength and $c_s \approx 3484\,{\rm m.s}^{-1}$ is the sound speed in the substrate in the z direction [50]. The aperture of the IDT is 2 cm. The amplitude of the acoustic wave was measured with a Mach-Zender interferometer. The substrate surface was treated by a self-assembled monolayer (SAM) of OTS (octadecyltricholorisilane), making it hydrophobic (static contact angle of 98°) and with weak contact angle hysteresis (15°). To avoid the acoustic wave reflection by the edge of the substrate, an

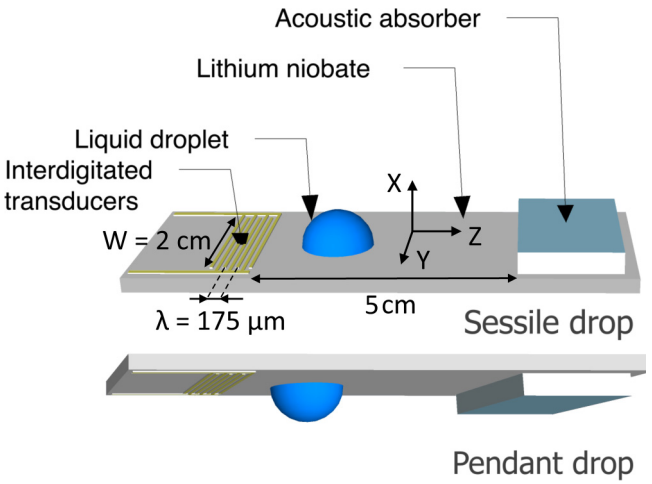

FIG. 2. Sketch of the experimental setup. A sessile drop of deionized water is excited with a Rayleigh surface acoustic wave of frequency 20 MHz synthesized at the surface of a x-cut niobate lithium substrate along the z axis. The wavelength λ and the aperture of the IDT W are, respectively, equal to 175 μm and 2 cm.

acoustic absorber (Blu-tack "UHU patafix") was placed at the extremity of the substrate, 5 cm away from the IDT in the propagation direction.

In sessile drop experiments, a droplet of calibrated volume is deposited on the top surface of the substrate corresponding to the active one. In pendant drop experiments, the setup is put upsidedown. Then waves are emitted and the droplet dynamics is recorded with a high speed camera (Photron SA3) with appropriate optics to obtain a close enough magnification of the drop. Finally, the drop oscillations and displacement, as well as the contact line dynamics, are analyzed with ImageJ software (see movies 1 and 2 in the Supplemental Material [51] illustrating the typical dynamic of a sessile and a pendant drop). The drop temperature evolution was not monitored in the present experiments since it was shown in previous studies [13–17] that water drop heating induced by SAW at this frequency and power is weak and that the characteristic timescale associated with the temperature increase is significantly larger than the characteristic timescale of our experiments (≈0.5 s).

B. Relevant dimensionless numbers

The relevant dimensionless number in this study are the Bond number Bo and the acoustical Weber number $We_{\rm ac}$.

The Bond number ${\rm Bo} = \rho_l g L^2/\sigma$ compares capillary effects to gravity effects, with ρ_l the density, g the standard gravity, L the characteristic size of the system, and σ the surface tension. In the case of a droplet, the characteristic length L corresponds to the radius of the drop at rest R_o and the Bond number quantifies the ability of gravity to deform droplets (departure from spherical shape imposed by surface tension). In the present experiments, we considered droplets of 2, 5, 10, and 15 μl corresponding to radii of $R_o \approx (3\mathcal{V}/2\pi)^{1/3}$ equal to 1.0, 1.3, 1.7, and 1.9 mm, respectively (if we consider that the drop are perfectly hemispherical) and thus Bond number Bo of, respectively, 0.13, 0.24, 0.38, and 0.5. Since the Bond number is small and the contact angle is around

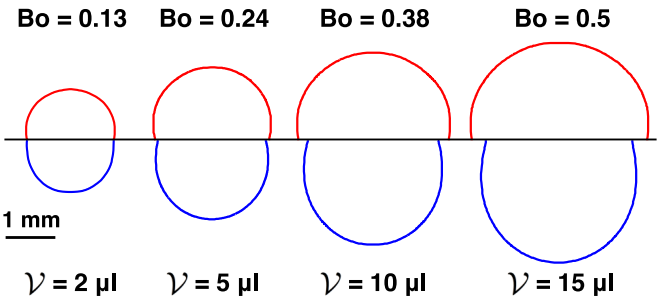

FIG. 3. Comparison of the initial static shape of sessile (up) and pendant (down) drops of volume 2 μl, 5 μl, 10 μl, and 15 μl (corresponding to Bond numbers of 0.13, 0.24, 0.38, and 0.5, respectively) deposited on the niobate lithium substrate treated with OTS.

90°, the adhesion forces are dominant over gravity and the drop remains attached to the substrate in the pendant case. Figure 3 compares the shape of these drops at rest when they are pendant and sessile corresponding to the reversal of the gravity field. For the four volumes considered, the relative deformation spans between 4.5% and 18% of the drop initial height, giving a direct measurement of the static effect of gravity for the four drop volumes considered.

The acoustical Weber number $\mathrm{We_{ac}}$ compares the acoustic radiation pressure to the capillary effects at the drop surface. This number, initially introduced in the study of acoustic levitation [52] or acoustically induced atomization [11], characterizes the ability of acoustic waves to deform interfaces, which shape is maintained by surface tension. For a droplet excited by SAWs, the air-water interface is almost a perfect mirror for the wave and the radiation pressure p_r can be estimated (in normal incidence) as $p_r \approx 2\langle e_{\mathrm{ac}}\rangle$, where e_{ac} is the acoustic energy density of the incident acoustic wave in the liquid [53] and the brackets $\langle\rangle$ correspond to time averaging. In the plane-wave approximation, the acoustic energy is equally distributed between potential and kinetic energy and in space, so $\langle e_{\mathrm{ac}}\rangle = 2\langle e_c\rangle$ with e_c the kinetic energy density. Then, considering a harmonic acoustic wave, we have $\langle e_c\rangle = 1/2\rho_l V_l^2$, where V_l is the amplitude of the acoustic velocity perturbation in the liquid and ρ_l the liquid density. Finally, since the acoustic wave is radiated in the liquid with the Rayleigh angle θ_R, continuity of the velocity field at the substrate-drop interface gives: $V_l = A_s\omega_{\mathrm{ac}}/\cos(\theta_R)$, where A_s is the amplitude of the normal acoustically induced displacement at the surface of the substrate, and ω_{ac} is the frequency of the acoustic wave. Finally, the Laplace law gives the order of magnitude of the pressure drop at the interface due to capillary effects: $p_{\mathrm{cap}} \approx 2\sigma/R$ with σ the liquid surface tension. As a consequence, the acoustical Weber number can be estimated according to the formula: $\mathrm{We_{ac}} = p_r/p_{\mathrm{cap}} = \rho_l A_s^2\omega_{\mathrm{ac}}^2 R/\sigma\cos^2(\theta_R)$. In this study we explored $\mathrm{We_{ac}}$ ranging from 0.2 to 0.6.

III. COMPARISON OF THE DYNAMICS OF SESSILE AND PENDANT DROPS: EFFECT OF GRAVITY

The observation of the dynamics of sessile droplet excited by traveling surface acoustic waves (see movie 1 in the Supplemental Material [51]) might give the misleading impression that during an oscillation cycle, the droplet is stretched by the effect of the wave (radiation pressure) and then falls down due to gravity. A previous study by Brunet *et al.* [3] has shown that the drop frequency f_{osc} depends on the drop volume $\mathcal{V}$ with a power law $f_{\mathrm{osc}} \sim \mathcal{V}^{-1/2}$, which is typical for Rayleigh-Lamb inertiocapillary vibration modes [54,55] (a gravity-based restoring force would have led to a $\mathcal{V}^{-1/6}$ power law; see, e.g., Ref. [56]). We can conclude from these results that capillary effects are dominant over gravity ones (as expected at such moderate Bo). Nevertheless, if gravity effects were negligible, dynamics of sessile and pendant drops should be strictly identical. We will show in the following that while it would be the case if the droplet was a linear oscillator, gravity strongly affects the drop dynamics due to nonlinearities. More generally, we will show that independently of its origin (external field, dynamically induced), the average drop stretching dramatically modifies the drop response. Before exploring this subject, we will first identify some specific regimes where the comparison between sessile and pendant drop dynamics is not relevant. Then we will compare the dynamics of oscillation and translation of sessile and pendant drops.

A. Specific regimes for pendant drops

When pendant drops are stretched above a critical threshold during their oscillation cycle, they detach from the surface, whereas sessile drops always remain attached to the substrate at the acoustic powers investigated in this paper. Interestingly, some new regimes of oscillation and displacement appear close to this threshold. We will first identify and analyze these regimes.

1. Phase diagram

The different droplet dynamics observed for pendant drops are summarized in the phase diagram of Fig. 4. For *low* $\mathrm{We_{ac}}$ (blue region), the droplet always remains attached to the surface and undergoes coupled oscillatory and translational motions similar to the one observed for sessile droplet at the same acoustic power. In the *intermediate region* (green), small variations in the experimental conditions can either lead to the detachment of the drop or to its sticking to the walls. This high sensitivity to experimental initial conditions is especially evident for droplets of 5 μl (corresponding to Bo = 0.24): for the same control parameters and after a similar transient regime, the droplet either experiences large oscillations leading to its detachment from the surface or small oscillations with larger translation speed (diamonds in Fig. 4 and depicted in Fig. 5). Finally, for *high* $\mathrm{We_{ac}}$ detachment always occurs.

It is interesting to note that a peculiar regime is observed for the biggest drop (15 μl, Bo = 0.5) close to the detachment threshold (triangles on Fig. 4). In this regime, the droplet reaches an equilibrium state with extremely small oscillations and slow velocity. The drop shape is quasiaxisymmetric (explaining why there is no translation) and the drop stretching remains close to the detachment threshold (see Fig. 6 and movie 3 in the Supplemental Material [51]).

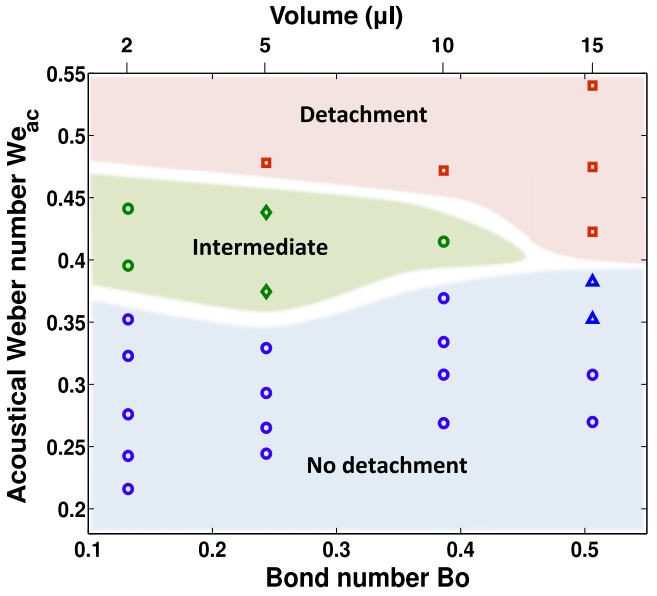

FIG. 4. Phase diagram as a function of We_{ac} and Bo summarizing the different regimes observed experimentally when pendant drops are excited by SAW. Blue region: no droplet detachment from the surface. Green region: intermediate region with either detachment or sticking of the drop to the surface. Red region: systematic drop detachment. Four drop dynamics are observed: dynamics similar to sessile drop (circle), detached drop (square), and new dynamics close to the detachment threshold for 5-μl drops (diamond, described in Fig. 5) and 15-μl drops (triangle, described in Fig. 6).

2. *Detachment*

Droplet detachment from the substrate is illustrated on Fig. 7. At first the drop is stretched vertically forming a quasicylindrical liquid column. Then the base of the drop is squeezed and pinches off. It is well known since the work of Savart [57], Plateau [58], and Rayleigh [54,59] that liquid columns are unstable to the Rayleigh-Plateau instability. Savart was the first to observe the decay of liquid jet into drops. Then Plateau has shown that surface tension favors the development of long wavelength undulations at the surface of a liquid

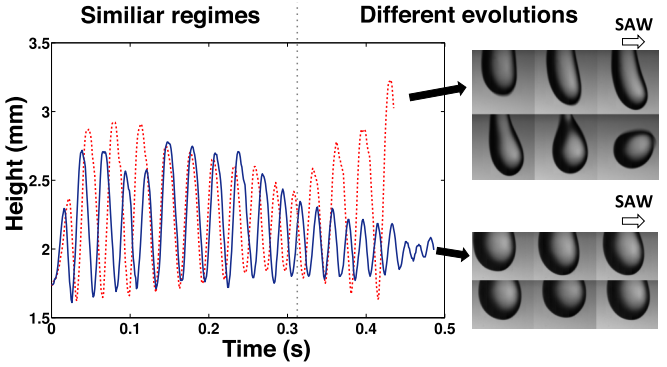

FIG. 5. Evolution of the drop height for two droplets of the same size (Bo = 0.24) excited with the same acoustical signal (We_{ac} = 0.44). The drop can either detach from the substrate (dashed line) or reach a stable regime with small oscillations and larger translation speed (solid line).

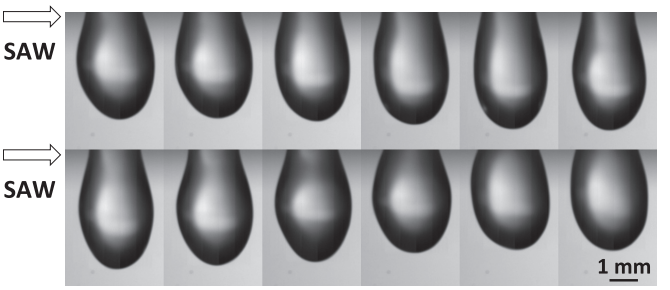

FIG. 6. Sequence of images (time elapsed between successive images: 4 ms, captured at 250 fps) of a drop of volume 15 μl (Bo = 0.5) excited with an acoustic power corresponding to $We_{ac} = 0.38$. The drop reaches a stable regime with large deformation but almost no oscillation and translation.

column since they reduce its free surface energy. Nevertheless, an analysis based solely on surface tension would predict the formation of the largest droplets (since they minimize the surface energy) while this is not observed in practice. Later on, Rayleigh demonstrated that surface tension has to work against inertia to induce jet breakup. With a stability analysis, he proved that the most unstable perturbations corresponds to wavelength $\lambda_R \approx 9R_j$ and that the characteristic time associated with this instability is $T_R = 2.91\sqrt{\frac{\rho_l R_j^3}{\sigma}}$ with R_j the liquid jet radius, σ the surface tension, and ρ_l the liquid density. In the present experiments, we measured the critical aspect ratio h_c/R_c of the liquid column during the last oscillation before breakup occurs (h_c and R_c are, respectively, the critical height and radius of the liquid column before breakup occurs).

The critical height (h_c) and radius (R_c) were measured during the cycle preceding the detachment when the droplet shape is the closest to a cylinder (minimal variation of the drop radius along the stretching axis). R_c is the average value of the cylinder radius along the stretching axis and h_c the drop height. Since the shape is not perfectly cylindrical, the error bars represent the minimum and maximum values of R_c along the stretching axis. Independently of the initial drop volume, we found that droplet detachment occurs when $h_c/R_c \approx 4.5$ (i.e., $\lambda_R/2$) (see Fig. 8). The same tendency was observed in Ref. [10] for focused SAWs. An interesting point is that the development of Rayleigh-Plateau instability requires not

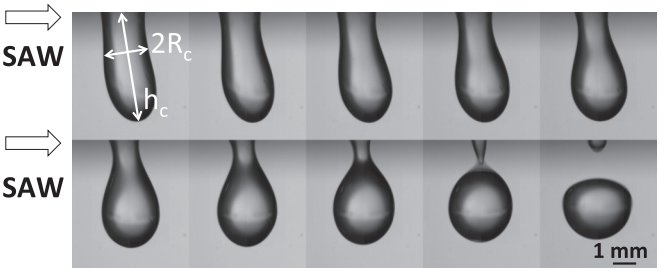

FIG. 7. Sequence of images (time elapsed between successive images: 2 ms, captured at 500 fps) showing the detachment of a drop of 10 μl excited with an acoustic power corresponding to We_{ac} = 0.41. The parameters h_c and R_c are, respectively, the critical height and radius of the liquid column before breakup occurs.

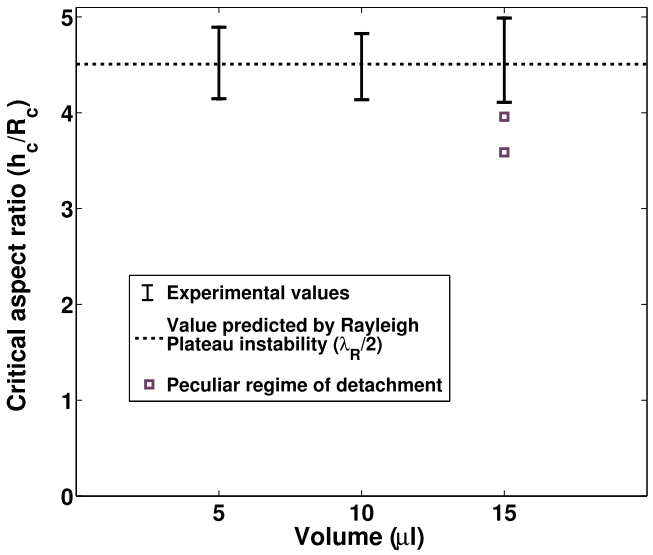

FIG. 8. Critical aspect ratio h_c/R_c leading to the drop detachment from the surface for different initial volumes. Square symbols correspond to the peculiar regime shown in movie 4 in the Supplemental Material [51].

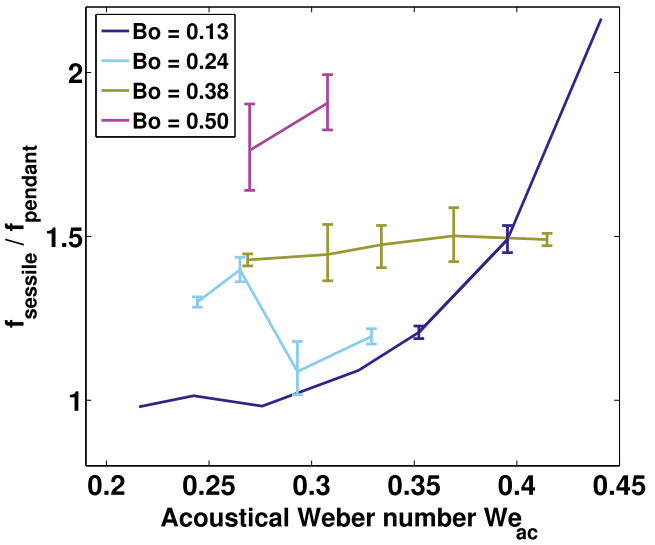

FIG. 9. Ratio between sessile and pendant drops oscillation frequencies $f_{\text{sessile}}/f_{\text{pendant}}$ as a function of We_{ac} for different Bond numbers Bo (corresponding to different droplet sizes). The error bars correspond to the variation of this ratio for the four experiments performed (two for sessile drops, two for pendant drops). When no error bars appear, the data point corresponds to the ratio between two measurements for sessile and pendant drops.

only a sufficient drop elongation but also a long enough time for the instability to develop. But since drop oscillations are inertiocapillarity oscillations, their period also scale as $\sqrt{\frac{\rho_l R_j^3}{\sigma}}$, which means that the two phenomena (instability and drop oscillations) have comparable characteristic times in the invicid regime.

As we can see in Fig. 8, two detachments deviate from the value predicted by the theory. Those points correspond to the peculiar regime presented in Fig. 6 but for a slightly higher We_{ac}. In this case, droplets experience stable oscillation during a long time and finally detach in a quasistatic way (see movie 4 in the Supplemental Material).

B. Droplet oscillatory motion

Now we can compare the dynamics of sessile and pendant drops away from these specific regimes. In this case, droplets remain attached to the substrate and undergo both oscillations and a translational motion. In this subsection we will focus on the effect of gravity on droplet quadrupolar oscillations. In the next subsection we will investigate the droplet translational motion.

A direct comparison of the quadrupolar oscillations for sessile and pendant drops at the same driving parameters shows that f_{osc} is always higher in the first case than in the second one (see Fig. 9), when the drop static deformation induced by gravity and/or the acoustic wave is significant. This ratio remains close to one only for the smallest Bond number ($\text{Bo} = 0.13$) where the static deformation induced by gravity is very small and for the smallest acoustic power $\text{We}_{\text{ac}} < 0.3$. It is interesting to note that even at small initial Bond number gravity can dramatically affect the oscillatory dynamics of the drop (factor up to 2 on f_{osc}) when it experiences large deformations (at large We_{ac}).

1. Theoretical analysis

To understand this behavior, we will consider that droplet vibrations can be described by an oscillator equation. This has been demonstrated for the eigen modes of levitating droplets [60–62] and sessile droplets with pinned contact lines [63,64]. The extension of such equations to sessile droplet with moving contact lines would require to properly include the dissipation in the vicinity of the triple line [65]. For small oscillations of the drop, the associated oscillator equation is linear and thus gravity does not affect its eigenfrequency but only its equilibrium position. Indeed, if we consider a harmonic oscillator submitted to the effect of gravity: $m\ddot{x} = -kx + mg$ (with k the spring stiffness, m the mass of the system and g the standard gravity) and introduce the natural angular frequency of the system $\omega_o = \sqrt{\frac{k}{m}}$, a simple change of variables $X = x - x_s$ with $x_s = g/\omega_o^2$ the static equilibrium position gives:

$$\ddot{X} + \omega_o^2 X = 0,$$

showing that the natural frequency ω_o is not affected by the external constant force field mg. Nevertheless, it has been proved [61,62,65] that droplets are nonlinear oscillators with quadratic nonlinearities when they undergo finite amplitude oscillations. These nonlinearities are due to the convective nonlinearity of Navier-Stokes equations but also to the nonlinearities associated with the interface deformation.

For the sake of simplicity and to qualitatively illustrate the effect, we will first consider an oscillator with a simple quadratic nonlinearity αx^2 submitted to a constant force field mg: $\ddot{x} + \omega_o^2(1 + \alpha x)x = g$, with α the nonlinearity coefficient. If we introduce as previously the static equilibrium position x_s, solution of the equation $x_s + \alpha x_s^2 = g/\omega_o^2$, and make the

substitution, $X = x - x_s$, we get

$$\ddot{X} + \omega_o^2(1 + 2\alpha x_s + \alpha X)X = 0. \quad (1)$$

In this case, we clearly see that both the static external force field mg (leading to a shift of the equilibrium position x_s) and dynamical effects affect the eigenfrequency of the system. We will analyze these two effects separately. If we consider tiny oscillations of the system $X \ll x_s$, around x_s, the eigen frequency of the system ω_s becomes $\omega_s^2 = \omega_o^2(1 + 2\alpha x_s)$, which is to say for moderate droplet deformation $\alpha x_s \ll 1$:

$$\omega_s = \omega_o(1 + \alpha x_s).$$

From a physical point of view, the effect of the external force field is clear: since the string is nonlinear and depends on the oscillator stretching, the gravity field simply modifies the equilibrium position of the system and thus its eigenfrequency.

To understand the role of dynamical effects, we can consider the situation when $x_s \ll X$. In this case, Eq. (1) becomes simply the one of a nonlinear oscillator with quadratic nonlinearities:

$$\ddot{X} + \omega_o^2(1 + \alpha X)X = 0.$$

This problem is treated in Landau textbook [66]. Poincaré expansion of X: $X = \epsilon X_1 + \epsilon^2 X_2 + \epsilon^3 X_3$, with $X_1 = A\cos(\omega_d)$ and $\omega_d = \omega_o + \epsilon\omega_1 + \epsilon^2\omega_2$, gives

$$X_2 = -\frac{\alpha A^2}{2} + \frac{\alpha A^2}{6}\cos(2\omega_d t).$$

We obtain the classical result that a quadratic nonlinearities leads to a static deformation $x_d = -\alpha A^2/2$ and oscillations at frequency $2\omega_o$. With this asymptotic expansion, we can also compute the eigen frequency shift induced by nonlinear effects: $\omega_d = \omega_o(1 + 5/6\,\alpha x_d)$.

Now, if we combine the effects of the stationary force field and dynamical effects we simply obtain: $\omega_{\rm nl} = \omega_o[1 + \alpha(x_s + 5/6x_d)]$, where $\omega_{\rm nl}$ is the eigen frequency of the nonlinear oscillator. It is interesting to note that both effects depend on the average stretching of the spring-mass system. Nevertheless, while the frequency shift induced by a steady external force field is independent of the amplitude of oscillation of the system, the frequency shift induced by dynamical effects is proportional to A^2 (since $x_d \propto A^2$).

The same method applies to the nonlinear equation describing drop quadrupolar oscillations [62]:

$$\ddot{x} + 2\lambda\dot{x} + \omega_o^2 x + \alpha\omega_o^2 x^2 + \beta\dot{x}^2 + \gamma x\ddot{x} = 0. \quad (2)$$

In this case, proper analysis (see the Appendix) shows that

$$\omega_{\rm nl} = \omega_o[1 + (\alpha - \gamma/2)x_s + K x_d], \quad (3)$$

where K is a complex function of the nonlinear coefficients α, β, and γ, and $x_d \propto A^2$. Of course, this analysis holds for weakly nonlinear systems. For larger nonlinearities, the dependence of the eigen frequency over the average drop stretching might be more complex than a simple linear shift.

2. *Experimental results*

The dependence of the eigenfrequency $f_{\rm osc}$ on its average stretching $h_m = 1/T\int_0^T h(t)dt$ has been measured for different acoustical power and droplet sizes (see Fig. 10).

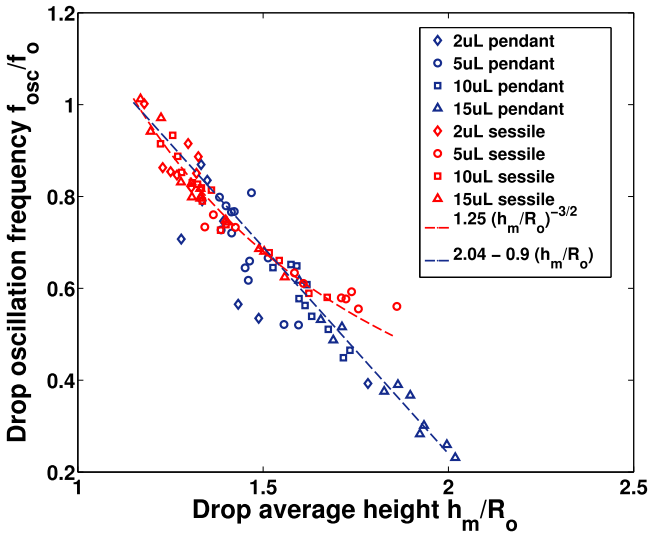

FIG. 10. Eigen frequency $f_{\rm osc}$ divided by the Rayleigh-Lamb frequency f_o as a function of the drop average height h_m divided by the drop static radius $R_o = (3V/2\pi)^{1/3}$ in the absence of gravity effects for different drop volumes and acoustical powers.

When $f_{\rm osc}$ divided by $f_o = 1/2\pi\sqrt{8\sigma/\rho_l R_o^3}$ (predicted by Rayleigh-Lamb theory) is plotted as a function of h_m divided by $R_o = (3V/2\pi)^{1/3}$ (the drop radius in absence of gravity effects), all data collapse into a single curve for both sessile and pendant drops as expected from previous analysis [67]. Nevertheless, the power law differs in these two cases. Data points are well fitted by a linear law for pendant drops ($f_{\rm osc}/f_o \approx 2.04 - 0.9h_m/R_o$) and by a power law $f_{\rm osc}/f_o = 1.25(h_m/R_o)^{-3/2}$ for sessile ones.

To determine which effects are responsible for the drop stretching (external force field or dynamical effects), we plotted the dimensionless average droplet stretching h_m/R_o as a function of the droplet amplitude of oscillation $\Delta h/R_o$ (see Fig. 11). For pendant drops no correlation between these two parameters is observed (except for the smallest drops of 2 μl), while for sessile droplets, a power law $h_m/R_o \approx 1.25 + 0.21(\Delta h/R_o)^2$ is obtained as expected from previous analysis when dynamical effects are dominant. Thus, these experiments show that the average drop stretching is mainly caused by stationary external force fields in the case of pendant drop, whereas dynamical effects induced by large amplitude oscillations are dominant for sessile drops. Indeed, in the first case, gravity and the radiation pressure induced by the acoustic field act in the same direction and lead to large h_m. For sessile drops, however, they act in opposite directions, and the average deformation induced by the drop oscillations and nonlinearities becomes dominant. Of course, for the smallest Bo (tiniest drops) the same evolution is observed for sessile and pendant drops since in this case gravity forces are negligible compared to capillary effects.

With these experimental results we can now explain the trends observed on Fig. 9. A higher frequency for sessile drops at constant $\rm We_{ac}$ is simply the result of smaller averaged deformations compared to those of pendant drops, which lead to a smaller frequency shift induced by nonlinear effects.

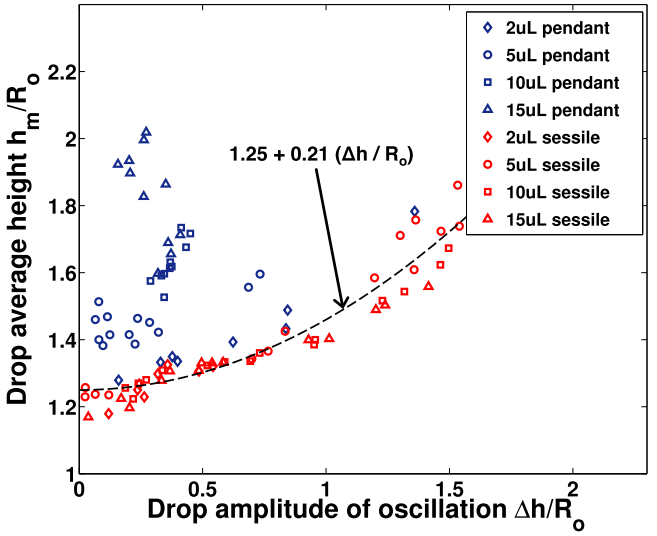

FIG. 11. Drop average height h_m as a function of the drop amplitude of oscillation Δh both divided by $R_o = (3V/2\pi)^{1/3}$, the drop static radius in absence of gravity. Only data for sessile drops show clear correlation between both quantities.

In conclusion, gravity acts indirectly on the drop oscillation frequency through the nonlinearities of the drop vibrations. The frequency shift can be significant (factor up to 2.5) even at moderate Bond numbers. Moreover, inverting the gravity field does not only affect the value of the eigen frequency, but also its dependance over the amplitude of the drop oscillations.

Finally, an interesting result is that it is possible to collapse all data obtained for both pendant and sessile droplets, different acoustical powers and droplet sizes by simply replacing the radius by the average height h_m in Rayleigh-Lamb formula (see Fig. 12). It simply means that the characteristic length for

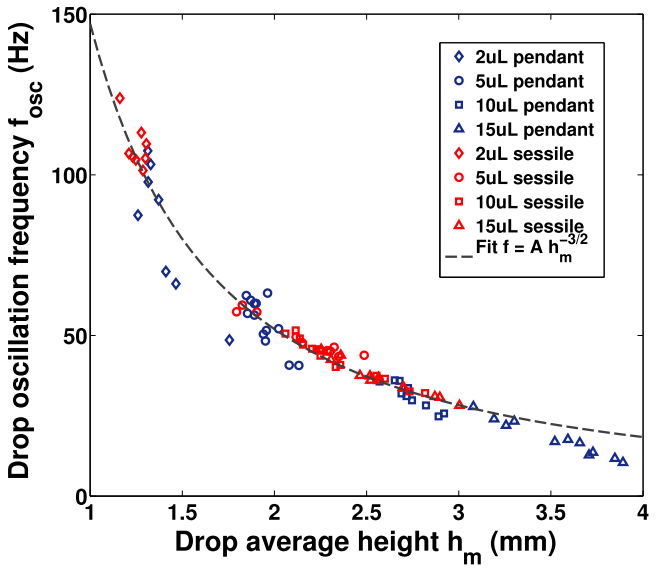

FIG. 12. Drop oscillation frequency as a function of the drop average height h_m for sessile (red) and pendant (blue) drop of different volumes, and different driving acoustical power. All data collapse into a single trend close to the power law predicted by the Rayleigh-Lamb theory.

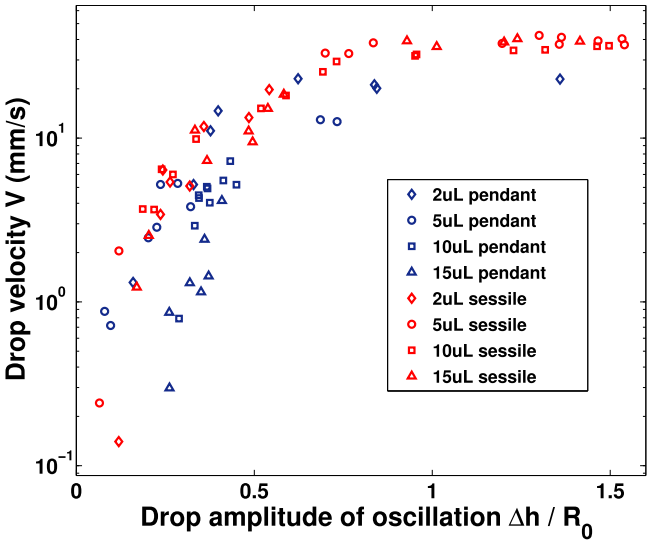

FIG. 13. Sessile (red or gray) and pendant (blue or black) drops translation speed as a function of the dimensionless amplitude $\Delta h/R_o$. The droplet velocity is measured from the side views of the drop motion by monitoring the position of the contact line and applying a low pass filter to suppress the effect of the drop oscillations.

the computation of stretched droplets eigen frequency is no longer the drop radius but instead their average height.

C. Droplet translational motion and correlation with the oscillations

When a droplet is excited by traveling surface acoustic waves, it moves in the same direction as the wave. This translation is due to the asymmetry of the acoustic field radiated in the drop along Rayleigh angle (given by Snell-Descartes law), which induces asymmetric deformation of the drop and thus different contact angles at the front and rear parts of the drop contact line.

In a recent paper, we have shown that there is a strong correlation [48] between droplet translational and oscillatory motion of sessile droplet. This correlation is represented on Fig. 13 for sessile and pendant drops. The good collapse of the data for sessile droplet and the smallest pendant drops (2 μl and 5 μl) indicates that in these cases, the amplitude Δh is the main quantity ruling its translational velocity. Whereas at higher volume (10 μl and 15 μl) pendant drop velocities V deviate from this correlation. It is also interesting to note that the translational velocity increases rapidly for drop oscillation $\Delta h/R_o < 0.3$ and then a saturation occurs for larger oscillations.

To understand this trend, we investigated the motion of the contact line during an oscillation cycle for both pendant and sessile drops. Indeed, V can be seen as the product of $f_{\rm osc}$ times the net displacement per cycle D.

Figure 14 compares the time-evolution shapes for sessile and pendant drops during a period at the same acoustic power, for the same drop size and for the same oscillation amplitude (see also movie 5 in the Supplemental Material [51]). For sessile drops, the contact line at the rear and that at the front move alternatively forward during the drop stretching and flattening (with much smaller displacement of

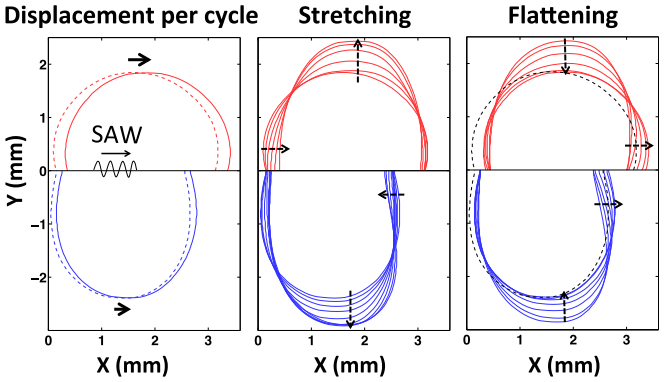

FIG. 14. Sessile (top) and pendant (bottom) drop shape evolution during an oscillation cycle. Left: initial and final shape. Center: shape evolution during the drop stretching phase. Right: shape evolution during the flattening phase.

the opposite contact line). However, for pendant drops, forward displacement of the rear contact line essentially occurs during the drop elongation while the front contact line first moves backward and then forward. This picture is representative of most of the cycles observed for different acoustical powers and droplet sizes.

Then, we analyzed the relation between the net motion of the front contact line during the drop extension and flattening as a function of $\Delta h/R_o$ (see Fig. 15). The contact line displacement per period is essentially a linear function of the amplitude of oscillation during both the stretching (backward movement of the contact line) and the flattening (forward movement of the contact line). Sessile and pendant drops front contact lines displacement have the same dependency on the amplitude of oscillation during the stretching phase but as seen on Fig. 15, the backward motion is smaller at same amplitude of oscillation for sessile drops. Since the frequency of oscillation is also smaller for pendant drops at the same amplitude of oscillation, it explains why pendant droplet velocity is always smaller as observed on Fig. 13.

IV. SEMIEMPIRICAL LAW AND ORIGIN OF THE SATURATION FOR SESSILE DROPS

The translational velocity for sessile drops under SAW excitation is strongly correlated to the amplitude of oscillation (see Fig. 13 and Ref. [48]). Nonetheless, no clear explanation of the relation between these quantities has been drawn, especially for the saturation at high oscillation amplitude. In the previous section we decompose the drop velocity as the product of the net displacement per cycle D times the drop oscillation frequency $f_{\rm osc}$: $V = D \times f_{\rm osc}$. On the one hand, we have shown that D is essentially a linear function of the drop amplitude of oscillation (Fig. 15). On the other hand, drop frequency in the sessile case is governed by dynamical nonlinear effects and is related to the mean deformation (Fig. 10) induced by amplitude of oscillation (Fig. 11). Those results can be summarized by the following relations:

(1) $D = K_1 \times \Delta h/R_o + K_2$,
(2) $f_{\rm osc}/f_o = K_3(h_m/R_o)^{-3/2}$,
(3) $h_m/R_o = K_4 + K_5(\Delta h/R_o)^2$,

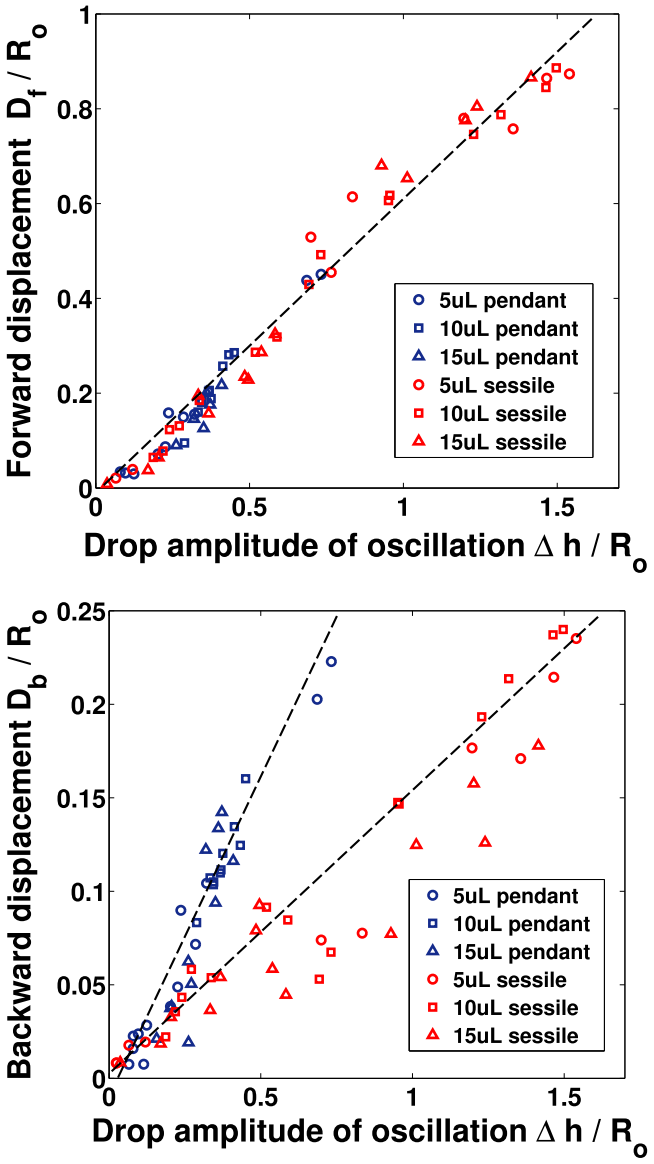

FIG. 15. Forward (up) and backward (down) displacement of the front part of the contact line of sessile (red or gray) and pendant (blue or dark) drops as a function of the dimensionless amplitude of oscillation $\Delta h/R_o$. The backward and forward displacements per cycle are calculated by monitoring the extreme positions of the contact line over one oscillation cycle, subtracting them to obtain the forward and backward displacements and averaging them over all the cycles in the stable regime.

with the coefficients $K_1 = 0.50$, $K_2 = 0.02$, $K_3 = 1.25$, $K_4 = 1.25$, and $K_5 = 0.21$ determined experimentally. If we combine these relations, we obtain

$$\frac{V}{V_o} = C_1\left[\frac{\Delta h}{R_o} + C_2\right] \times \left[1 + C_3\left(\frac{\Delta h}{R_o}\right)^2\right]^{-3/2}, \qquad (4)$$

with $V_o = f_o R_o$ the characteristic velocity associated with droplet oscillation, $C_1 = K_1 K_3 K_4^{-3/2} \approx 0.45$, $C_2 = K2/K_1 \approx -0.04$, and $C_3 = K_5/K_4 \approx 0.17$.

The predictions obtained with Eq. (4) are compared to experimental data on Fig. 16. The trends are globally recovered

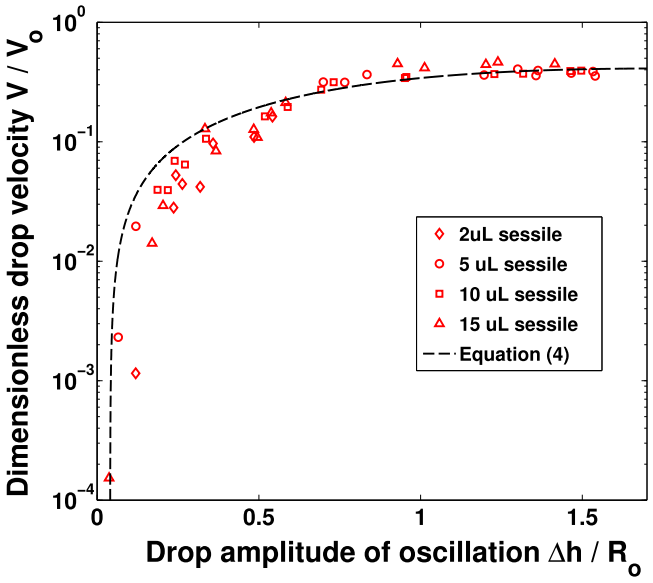

FIG. 16. Dimensionless sessile droplet translation speed V/V_o as a function of the drop amplitude of oscillation $\Delta h/R_o$, with $V_o = f_o R_o$ the characteristic velocity associated with droplet oscillations and $R_o \approx (3\mathcal{V}/2\pi)^{1/3}$ the drop static radius in absence of gravity. Dashed line: Eq. (4).

even if a weak discrepancy is observed for intermediate amplitude oscillations. These differences come from the fact that the net motion per period is not perfectly a linear function of Δh. Nevertheless, this comparison allows us to understand that the saturation of the droplet velocity is due to the decrease of f induced by dynamical nonlinear effects.

V. CONCLUSION

In this paper, we have analyzed the effect of gravity on the dynamics of drops excited by SAWs but also clarified the link between droplets oscillations and their translational motion. Further investigations using different contact angles and hysteresis would be of interest to get a deeper insight into the relation between drop oscillation and contact line mobility. Moreover, as underlined in a recent review [46], another great challenge is to unveil the origin of the drop oscillations and establish the missing link between the high-frequency (∼20 MHz) acoustic excitation and the low-frequency (∼50 Hz) droplet oscillatory response.

ACKNOWLEDGMENTS

This work was supported by grants from the Agence Nationale de la Recherche (Grant No. ANR-12-BS09-0021-01), the Direction Générale de l'Armement (France), and the Région Nord Pas-de-Calais.

APPENDIX

Oscillating droplets can be modeled by the following nonlinear equation [62]:

$$\ddot{x} + 2\lambda\dot{x} + \omega_o^2 x + \alpha\omega_o^2 x^2 + \beta\dot{x}^2 + \gamma x\ddot{x} = 0. \qquad \text{(A1)}$$

To determine the frequency shift induced by a stationary force field, we follow the same approach as presented in Sec. III B. We introduce the equilibrium position $x_s + \alpha {x_s}^2 = g/{\omega_o}^2$ and then make the substitution $X - x_s$. Equation (A1) thus becomes

$$\ddot{X} + \frac{2\lambda}{1+\gamma(x_s+X)}\dot{X} + \frac{1+\alpha(2x_s+X)}{1+\gamma(x_s+X)}\omega_o^2 X + \frac{\beta}{1+\gamma(x_s+X)}\dot{X}^2 = 0.$$

We then assume that $X \ll x_s$; i.e., the drop oscillation is small compared to the static deformation. This hypothesis is supported by experimental observations on pendant drops (Fig. 11). Then, by neglecting the influence of the viscosity, we get

$$\ddot{X} + \frac{1+2\alpha x_s}{1+\gamma x_s}\omega_o^2 X = 0.$$

Finally, for small static deformations ($\gamma x_s, \alpha x_s \ll 1$), the frequency shift induced by a stationary force field is

$$\omega_s = \omega_o\left[1 + \left(\alpha - \frac{\gamma}{2}\right)x_s\right].$$

Drop frequency shift induced by large oscillations has been theoretically investigated by Tsamopoulos and Brown [61]: they showed that drop frequency evolves as $\omega_d = \omega_o(1 + K'A^2)$ with A the amplitude of oscillation, in good agreement with experiments [60].

Now following the Landau method used in Sec. III B, the differential equation ruling the time evolution of X_2 is

$$\ddot{X}_2 + \omega_o^2 X_2 = \tfrac{1}{2}\left(\alpha + (\beta-\gamma)\omega_o^2\right)A^2 - \tfrac{1}{2}\left(\alpha - (\beta-\gamma)\omega_o^2\right)A^2\cos(2\omega_d t).$$

By solving this equation, we obtain the following expression for X_2:

$$X_2 = \frac{\left[(\gamma-\beta)\omega_o^2 - \alpha\right]}{2\omega_o^2}A^2 - \frac{\left[\alpha - (\gamma+\beta)\omega_o^2\right]}{2\omega_o^2}A^2\cos(2\omega_d t).$$

We can then express the mean deformation induced by the nonlinearities of the equation (A1):

$$x_d = \langle X\rangle = \langle X_2\rangle = \frac{\left((\gamma-\beta)\omega_o^2 - \alpha\right)}{2\omega_o^2}A^2.$$

The frequency shift can now be expressed in terms of the average deformation:

$$\omega_d = \omega_o\left\{1 + K'\frac{2\omega_o^2}{\left[(\gamma-\beta)\omega_o^2 - \alpha\right]}x_d\right\} = \omega_o(1 + Kx_d).$$

Finally, since we perform weakly nonlinear analysis (through asymptotic expansion), the two effects can be added to obtain the drop nonlinear frequency:

$$\omega_{nl} = \omega_o[1 + (\alpha - \gamma/2)x_s + Kx_d].$$

[1] A. Wixforth, C. Strobl, C. Gauer, A. Toegl, J. Scriba, and Z. Guttenberg, Anal. Bioanal. Chem. **379**, 982 (2004).

[2] A. Renaudin, P. Tabourier, V. Zang, J. Camart, and C. Druon, Sensors Actuators B **113**, 389 (2006).

[3] P. Brunet, M. Baudoin, O. B. Matar, and F. Zoueshtiagh, Phys. Rev. E **81**, 036315 (2010).

[4] S. Collignon, J. Friend, and L. Yeo, Lab on a chip **15**, 1942 (2015).

[5] Y. Babetta and L. Marrone, Microfluid. Nanofluid. **13**, 715 (2012).

[6] S. Shiokawa, Y. Matsui, and T. Ueda, IEEE Ultrason. Symp. **1**, 643 (1989).

[7] S. Shiokawa, Y. Matsui, and T. Ueda, Jpn. J. Appl. Phys. **29**, 137 (1990).

[8] K. Chono, N. Shimizu, Y. Matsui, J. Kondoh, and S. Shiokawa, Jpn. J. Appl. Phys. **43**, 2987 (2004).

[9] A. Qi, L. Yeo, and J. Friend, Phys. Fluids **20**, 074103 (2008).

[10] M. K. Tan, J. R. Friend, and L. Y. Yeo, Phys. Rev. Lett. **103**, 024501 (2009).

[11] D. J. Collins, O. Manor, A. Winkler, H. Schmidt, J. R. Friend, and L. Y. Yeo, Phys. Rev. E **86**, 056312 (2012).

[12] T. Frommelt, M. Kostur, M. Wenzel-Schäfer, P. Talkner, P. Hänggi, and A. Wixforth, Phys. Rev. Lett. **100**, 034502 (2008)..

[13] J. Kondoh, N. Shimizu, Y. Matsui, M. Sugimoto, and S. Shiokawa, IEEE Ultrason. Symp. **2**, 1023 (2005).

[14] S. Ito, Y. Sugimoto, Y. Matsui, and J. Kondoh, Jpn. J. Appl. Phys. **46**, 4718 (2007).

[15] J. Kondoh, N. Shimizu, Y. Matsui, M. Sugimoto, and S. Shiokawa, Sensors Actuators A **149**, 292 (2009).

[16] J. Reboud, Y. Bourquin, G. Wilson, G. Pall, M. Jiwaji, A. Pitt, A. Graham, A. Waters, and J. Cooper, Proc. Natl. Acad. Sci. U.S.A. **109**, 15162 (2012).

[17] T. Roux-Marchand, D. Beyssen, F. Sarry, and O. Elmazria, IEEE Trans. Ultrason. Ferroelectr. Freq. Control **62**, 729 (2015).

[18] R. J. Shilton, V. Mattoli, M. Travagliati, M. Agostini, A. Desii, F. Beltram, and M. Cecchini, Adv. Funct. Mater. **25**, 5895 (2015).

[19] S. Girardo, M. Cecchini, F. Bletram, R. Cingolani, and D. Pisignano, Lab Chip **8**, 1557 (2008).

[20] M. Cecchini, S. Giardo, D. Psignano, R. Cingolani, and F. Beltram, Appl. Phys. Lett. **92**, 104103 (2008).

[21] W.-K. Tseng, J.-L. Lin, W.-C. Sung, S.-H. Chen, and G.-B. Lee, J. Micromech. Microeng. **16**, 539 (2006).

[22] M. Tan, L. Yeo, and J. Friend, Europhys. Lett. **87**, 47003 (2009).

[23] M. B. Dentry, J. Friend, and L. Yeo, Lab Chip **14**, 750 (2014).

[24] R. Shilton, M. Tan, L. Yeo, and J. Friend, J. Appl. Phys. **104**, 014910 (2008).

[25] J. Shi, X. Mao, D. Ahmed, A. Colletti, and T. Huang, Lab Chip **8**, 221 (2008).

[26] J. Shi, D. Ahmed, X. Mao, S.-C. S. Lin, and T. Huang, Lab Chip **9**, 2890 (2009).

[27] R. Raghavan, J. Friend, and L. Yeo, Microfluid. Nanofluid. **8**, 73 (2010).

[28] S. Tran, P. Marmottant, and P. Thibault, Appl. Phys. Lett. **101**, 114103 (2012).

[29] X. Ding, S.-C. S. Lin, B. Kiraly, H. Yue, S. Li, J. Shi, S. Benkovic, and T. Huang, Proc. Natl. Acad. Sci. U.S.A. **109**, 11105 (2012).

[30] J. Guo, J. Li, Y. Chen, L. Yeo, and J. Friend, IEEE Trans. Microwave Theory Tech. **62**, 1898 (2014).

[31] D. Collins, T. Alan, and A. Neild, Appl. Phys. Lett. **105**, 033509 (2014).

[32] T. Franke, S. Braunmuller, L. Schmid, A. Wixforth, and D. Weitz, Lab Chip **10**, 789 (2010).

[33] A. Hartmann, M. Stamp, R. Kmeth, S. Buchegger, S. Bernd, B. Saldamli, R. Bugkart, M. Schnieder, and A. Wixforth, Lab Chip **14**, 542 (2014).

[34] A. Bussonnière, Y. Miron, M. Baudoin, O. Bou Matar, M. Grandbois, P. Charette, and A. Renaudin, Lab Chip **14**, 3556 (2014).

[35] N. Sivanantha, C. Ma, D. Collins, M. Sesen, J. Brenker, R. Coppel, A. Neild, and T. Alan, Appl. Phys. Lett. **105**, 103704 (2014).

[36] X. Ding, Z. Peng, S.-C. S. Lin, M. Geri, S. Li, P. Li, Y. Chen, M. Dao, S. Suresh, and T. Huang, Proc. Natl. Acad. Sci. U.S.A. **111**, 12992 (2014).

[37] P. Li, Z. Mao, Z. Peng, L. Zhou, Y. Chen, P.-H. Huang, C. Truica, J. Drbick, W. El-Deiry, M. Dao, S. Suresh, and T. Huang, Proc. Natl. Acad. Sci. U.S.A. **112**, 4970 (2015).

[38] F. Guo, P. Li, J. French, Z. Mao, H. Zhao, S. Li, N. Nama, J. Fick, S. Benkovic, and T. Huang, Proc. Natl. Acad. Sci. U.S.A. **112**, 43 (2015).

[39] A. Riaud, J.-L. Thomas, E. Charron, A. Bussonnière, O. B. Matar, and M. Baudoin, Phys. Rev. Appl. **4**, 034004 (2015).

[40] A. Riaud, J.-L. Thomas, M. Baudoin, and O. B. Matar, Phys. Rev. E **92**, 063201 (2015).

[41] D. Baresch, J.-L. Thomas, and R. Marchiano, Phys. Rev. Lett. **116**, 024301 (2016).

[42] A. Riaud, M. Baudoin, J.-L. Thomas, and O. B. Matar, Phys. Rev. E **90**, 013008 (2014).

[43] L. Yeo and J. Friend, Biomicrofluidics **3**, 012002 (2009).

[44] J. Friend and L. Yeo, Rev. Mod. Phys. **83**, 647 (2011).

[45] X. Ding, P. Li, S.-C. S. Lin, Z. S. Stratton, N. Nama, F. Guo, D. Slotcavage, X. Mao, J. Shi, F. Costanzo, and T. J. Huang, Lab Chip **13**, 3626 (2013).

[46] L. Yeo and J. Friend, Annu. Rev. Fluid Mech. **46**, 379 (2014).

[47] D. Beyssen, L. Brizoual, O. Elmazria, and P. Alnot, Sensors Actuators B **118**, 380 (2006).

[48] M. Baudoin, P. Brunet, O. Bou Matar, and E. Herth, Appl. Phys. Lett. **100**, 154102 (2012).

[49] J. Blamey, L. Yeo, and J. Friend, Langmuir **29**, 3835 (2013).

[50] J. Campbell and W. Jones, IEEE Trans. Sonics Ultrason. **17**, 71 (1970).

[51] See Supplemental Material at http://link.aps.org/supplemental/10.1103/PhysRevE.93.053106 for movies showing the dynamics of sessile and pendant drops.

[52] W. Shi, R. Apfel, and R. Holt, Phys. Fluids **7**, 2601 (1995).

[53] F. Borgnis, Rev. Mod. Phys. **25**, 653 (1953).

[54] L. Rayleigh, Proc. R. Soc. London A **29**, 94 (1879).

[55] H. Lamb, *Hydrodynamics* (Cambridge University Press, England, 1932).

[56] M. Perez, Y. Brechet, L. Salvo, M. Papoular, and M. Suery, Europhys. Lett. **47**, 189 (1999).

[57] F. Savart, Ann. Chim. Phys. **53**, 337 (1833).

[58] J. Plateau, Mem. Ac. Roy. Sci **23**, 1 (1849).

[59] L. Rayleigh, Proc. London Math. Soc. **10**, 4 (1878).

[60] E. Trinh and T. G. Wang, J. Fluid Mech. **122**, 315 (1982).

[61] R. Tsamopoulos and R. A. Brown, J. Fluid Mech. **127**, 519 (1983).

[62] A. Bussonnière, Surface acoustic waves actuators for microfluidic: from underlying physics to biological applications, Ph.D. thesis, Université Lille 1, Villeneuve d'Ascq, 2014.

[63] J. B. Bostwick and P. H. Steen, J. Fluid Mech. **760**, 5 (2014).

[64] C.-t. Chang, J. B. Bostwick, S. Daniel, and P. H. Steen, J. Fluid Mech. **768**, 442 (2015).

[65] D. V. Lyubimov, T. P. Lyubimova, and S. V. Shklyaev, Phys. Fluids **18**, 012101 (2006).

[66] L. D. Landau and E. M. Lifshitz, *Mechanics*, 3rd ed. (Pergamon Press, Oxford, 1976).

[67] NB: Since the contact angle is slightly superior to $\pi/2$ and the Rayleigh-Lamb frequency is estimated for a levitating drop while it is sessile or pendant here, we do not have exactly $f/f_o \to 1$ when $h_m/R_o \to 1$.